Long-time properties of magnetohydrodynamic turbulence and the role of symmetries

Julia E. Stawarz,[1,2] Annick Pouquet,[1] and Marc-Etienne Brachet[3]

[1]*Geophysical Turbulence Program, Computational and Information Systems Laboratory, National Center for Atmospheric Research, P.O. Box 3000, Boulder Colorado 80307, USA*

[2]*Laboratory for Atmospheric and Space Physics, University of Colorado at Boulder, Boulder, Colorado, USA*

[3]*Laboratoire de Physique Statistique de l'École Normale Supérieure, associée au Centre National de la Recherche Scientifique et aux Universités Paris VI et VII, 24 Rue Lhomond, 75231 Paris, France*

(Received 9 April 2012; published 10 September 2012)

Using direct numerical simulations with grids of up to 512^3 points, we investigate long-time properties of three-dimensional magnetohydrodynamic turbulence in the absence of forcing and examine in particular the roles played by the quadratic invariants of the system and the symmetries of the initial configurations. We observe that when sufficient accuracy is used, initial conditions with a high degree of symmetries, as in the absence of helicity, do not travel through parameter space over time, whereas by perturbing these solutions either explicitly or implicitly using, for example, single precision for long times, the flows depart from their original behavior and can either become strongly helical or have a strong alignment between the velocity and the magnetic field. When the symmetries are broken, the flows evolve towards different end states, as already predicted by statistical arguments for nondissipative systems with the addition of an energy minimization principle. Increasing the Reynolds number by an order of magnitude when using grids of 64^3–512^3 points does not alter these conclusions. Furthermore, the alignment properties of these flows, between velocity, vorticity, magnetic potential, induction, and current, correspond to the dominance of two main regimes, one helically dominated and one in quasiequipartition of kinetic and magnetic energies. We also contrast the scaling of the ratio of magnetic energy to kinetic energy as a function of wave number to the ratio of eddy turnover time to Alfvén time as a function of wave number. We find that the former ratio is constant with an approximate equipartition for scales smaller than the largest scale of the flow, whereas the ratio of time scales increases with increasing wave number.

DOI: 10.1103/PhysRevE.86.036307 PACS number(s): 47.65.−d, 47.27.Gs, 47.27.ek, 94.05.Lk

I. INTRODUCTION

A. Context

Magnetic fields pervade the universe and often play an essential role in configuring and constraining structures, as in the case of intergalactic jets or closer to Earth in the solar wind or the magnetosphere. Magnetic pressure contributes to the containment of the heliosphere [1] and it may retard, together with turbulent pressure, the gravitational collapse of molecular clouds in the interstellar medium. Magnetic fields are also known to accelerate the motion of charged particles in the magnetospheres of the planets in the solar system, as in the case of Jupiter's aurora [2] (see Ref. [3] for the main characteristic of the auroral emissions as of today).

Such magnetic fields have been observed in a variety of media to be turbulent, such as in the solar wind [4] (see Ref. [5] for a recent review), in the interstellar medium where it is thought to be responsible for strong velocity shear and intermittency [6], or more recently in the heliosheath [7]. Using Cluster data with short separation between the satellites, it was shown in Ref. [8] that anisotropy of the energy Fourier spectra develops at small scales as predicted in weak magnetohydrodynamic (MHD) turbulence theory [9–11]. Solar wind turbulence can also help focus Langmuir wave packets that are routinely observed using Ulysses or Stereo spacecrafts [12].

Furthermore, magnetic fields can lead to extreme energetic events due to reconnection of magnetic field lines in highly turbulent media; solar flares are one such example, the prediction of which is one of the purposes of space weather research because of the disturbance to Earth's communication networks and power grids. The penetration of the solar wind into the Earth's magnetosphere can be explained by the development of Kelvin-Helmoltz (KH) vortices, as observed in Ref. [13], and a relationship between such KH instabilities and flux transfer events was found recently during substorms using multiple spacecrafts [14].

An understanding of both fluid and MHD turbulence has escaped us for a long time. Is MHD turbulence similar to hydrodynamic turbulence, with a Kolmogorov energy spectrum $E_K(k) \sim \epsilon^{2/3} k^{-5/3}$, with $\epsilon \equiv dE/DT$ the energy dissipation rate, perhaps with an anisotropy due to the presence of strong uniform fields of magnitude B_0? Or is it different, because Alfvén waves propagate that alter and dampen the nonlinear dynamics of turbulent flows, leading to a so-called Irsohnnikov-Kraichnan (IK) energy spectrum $E_{\rm IK}(k) \sim [\epsilon B_0]^{1/2} k^{-3/2}$? Further, is there one answer to these questions, or is universality broken in magnetohydrodynamics, as sometimes advocated? For example, it was found in Ref. [15] that one can observe three different energy spectra [Kolmogorov, IK, and weak turbulence (WT) $E_{\rm WT}(k_\perp) \sim k_\perp^{-2}$] for three different initial conditions of the magnetic field, using the same velocity field and with the same ideal invariants, namely, total energy, total magnetic helicity, and total cross correlation between the velocity and the magnetic field, with moreover no imposed external field, no forcing, unit magnetic Prandtl number, and equal kinetic and magnetic energies initially. In other words, for such a set of initial conditions, nothing allows for distinguishing these three configurations from a statistical point of view, no externally imposed time

scale is present, and the only constraint is that numerically the velocity and magnetic fields are forced to follow the fourfold symmetry of the initial conditions. Using this symmetry, one can gain in resolution and cost of computation and thus the Reynolds numbers are quite large (with the Taylor Reynolds number in excess of 1200), with equivalent resolutions of 2048^3 grid points. Similar results are found to hold in the forced case as well, for which long-time averaging is feasible [16].

The difference between these three power laws could be due to nonlocal interactions in Fourier space, between widely separated scales. Nonlocal interactions are thought to be more prevalent in magnetohydrodynamics than in hydrodynamics, as measured in high-resolution numerical simulations [17,18], and such nonlocality in Fourier space is advocated in the differentiation between a Kolmogorov and an IK spectrum, but what would make one of the three flows studied in Ref. [15] more nonlocal than others? Perhaps the different behaviors come from another factor. On the one hand, it could be that the ratio of kinetic to magnetic energy, in particular in the gravest mode, matters, as indicated in Ref. [15]. On the other hand, the invariants, which are quadratic in the basic fields, are identical but higher-order moments could differ; for example, it was shown in Ref. [19] that the skewness of one of the flows studied in Ref. [15] is measurably larger than that of the two other flows when looking at both the velocity and the magnetic field.

The assumption that with the same invariants, the three flows should behave in similar ways is based on an assumption of ergodicity. However, the ergodicity of turbulent flows has been put into question in a variety of contexts. It has been observed that long-time memory effects can be found in such flows, for example, in two-dimensional MHD turbulence [20], where large bursts of energy were observed to evolve on time scales of the order of 100 turnover times; it was also found more recently in numerical simulations of three-dimensional (3D) hydrodynamic turbulence [21] and in laboratory experiments (see, e.g., Ref. [22] and references therein). In the atmospheric boundary layer, one observes that statistics can depend on the large scales; this may be related to averaging over regions with local fluctuations in Reynolds number [23]. Such a transfer between nonlocal triads is shown to lead, however, to local exchanges of energy in hydrodynamics [24].

The persistence of modes for long times in magnetohydrodynamics, associated with large-scale coherent structures, was recently linked to normal modes appearing because of magnetic helicity, a large-scale invariant in the ideal case, and leading to an apparent breaking of ergodicity at the largest scale insofar as these structures persist for long times [25]. A similar phenomenon occurs for hydrodynamics in the presence of solid body rotation: Although the Coriolis force is linear, it affects the dynamics of rotating turbulence in slowing it down substantially [26]; this can be attributed to inertial waves, nonlinear transfer occurring only through resonances (or quasiresonances) [11].

In selective decay, some invariants are viewed as more sturdy than others; thus they may influence the long-term dynamics of decaying turbulent flows. This hypothesis is based on the fact that invariants may have different physical dimensions, for example, magnetic potential $\langle A^2\rangle$, with $\mathbf{b} = \boldsymbol{\nabla}\times\mathbf{A}$, and total energy $\frac{1}{2}\langle|\mathbf{v}|^2+|\mathbf{b}|^2\rangle$ in two dimensions or magnetic helicity $\langle\mathbf{A}\cdot\mathbf{b}\rangle$ and total energy in three dimensions: Since dissipation involves a Laplacian, it is thought that $\langle A^2\rangle$ or $\langle H_M\rangle$ will decay more slowly than energy. However, the third invariant in ideal magnetohydrodynamics, $H_C = \langle\mathbf{v}\cdot\mathbf{b}\rangle$, has the same dimension as energy and it could also influence the long-term dynamics, becoming strong in relative terms, that is, with respect to the energy, implying an alignment between the velocity and the magnetic field, a phenomenon called dynamic alignment. The relative importance of these two effects was explored both theoretically and numerically in Refs. [27,28] for random initial conditions. These theoretical considerations based on statistical mechanics of a truncated system of modes were backed up by rather low-resolution numerical simulations using a moderate number of Fourier modes; they nevertheless clearly demonstrated the validity of the approach: The end state of such flows was determined by the respective ratio of their three invariants. Will the same happen here, when starting with the three flows studied in Ref. [15], which statistically are equivalent but display different inertial range dynamics at peak of dissipation (and in the statistically steady state as well)? This is the main question that this paper is addressing, using direct numerical simulations of the MHD equations in three space dimensions.

B. Equations

We now give the MHD equations for an incompressible fluid with $\mathbf{v}$ and $\mathbf{b}$ respectively the velocity and magnetic fields in Alfvénic units:

$$\frac{\partial\mathbf{v}}{\partial t}+\mathbf{v}\cdot\boldsymbol{\nabla}\mathbf{v} = -\frac{1}{\rho}\boldsymbol{\nabla}\mathcal{P}+\mathbf{j}\times\mathbf{b}+\nu\nabla^2\mathbf{v}, \tag{1}$$

$$\frac{\partial\mathbf{b}}{\partial t} = \boldsymbol{\nabla}\times(\mathbf{v}\times\mathbf{b})+\eta\nabla^2\mathbf{b}; \tag{2}$$

$\rho = 1$ is the (uniform) density (and $\mathbf{b}$ is then dimensionally a velocity as well, the Alfvén velocity), $\mathcal{P}$ is the total pressure, $\boldsymbol{\nabla}\cdot\mathbf{v} = \boldsymbol{\nabla}\cdot\mathbf{b} = 0$, and ν and η are respectively the kinematic viscosity and magnetic diffusivity; we take $\nu = \eta$. With $\nu = 0$ and $\eta = 0$, the energy E_T, the cross helicity H_C, and the magnetic helicity H_M, defined as

$$E_T = E_V + E_M = \langle v^2+b^2\rangle/2,$$
$$H_C = \langle\mathbf{v}\cdot\mathbf{b}\rangle/2, \quad H_M = \langle\mathbf{A}\cdot\mathbf{b}\rangle/2,$$

are conserved. Relative helicities can be defined as follows:

$$\sigma_C = \cos[\mathbf{v},\mathbf{b}], \quad \sigma_M = \cos[\mathbf{A},\mathbf{b}], \quad \sigma_V = \cos[\mathbf{v},\boldsymbol{\omega}]; \tag{3}$$

they correspond to the degree of alignment between various vectors: the velocity, the magnetic field, the magnetic potential (with $\sigma_M = \pm 1$ defining a force-free field), or the vorticity (with $\sigma_V = \pm 1$ defining the so-called Beltrami configuration). In the latter case, the relative kinetic helicity involves the vorticity $\omega = \boldsymbol{\nabla}\times\mathbf{v}$; the total kinetic helicity is an invariant of the Euler equations ($\mathbf{b}\equiv 0$ and $\nu\equiv 0$).

The weakening of nonlinearities than can be diagnosed through the σ coefficients just defined is a topic that has received a great deal of attention through the years, starting with the fluid turbulence community; for example, it was shown in Ref. [29] that random flows have a natural (generic) degree of alignment, so that one must be careful in the interpretation of the data when considering the values reached

by the σ coefficients as to what can be attributed to pure randomness and what is due to the dynamics of the turbulent flow. It was also shown in Ref. [30] that vorticity stretching is accompanied by vorticity alignment with the intermediate eigenvector of the symmetrized velocity gradient matrix corresponding to the second eigenvalue λ_2, with $\lambda_1 > \lambda_2 > \lambda_3$ and $\lambda_1 > 0, \lambda_3 < 0$, because of incompressibility, suggesting that regions of dissipations are in the form of sheets.

Alignment and depression of nonlinearities also has its history in magnetohydrodynamics; for example, it was shown in Ref. [31], using two-dimensional direct numerical simulations (DNS) and models of magnetohydrodynamics, that the velocity and the magnetic field have a strong tendency to align, as also studied in Ref. [32]. More recently, the three-dimensional problem was tackled in Ref. [33], where clear alignment properties between all fields were obtained, including the induction and current, although in that latter case it does not correspond to an invariant but rather it of course reflects the weakening of the Lorentz force in the primitive equations. In fact, minimization principles using the ideal invariants of magnetohydrodynamics, dating back to Woltjer [34] (see Ref. [35] for the general case taking the three ideal invariants into account), predict such alignment tendencies for the vectors in the MHD equations.

The kinetic energy spectrum is the Fourier transform of the velocity two-point correlation function. Once homogeneity, isotropy, and incompressibility have been taken into account, only two defining functions remain: $E_V(k)$ is proportional to the kinetic energy, with $\int E_V(k)dk = E_V = \frac{1}{2}\langle v^2 \rangle$, and the kinetic helicity $H_V(k)$ stems from the antisymmetric part of the velocity gradient tensor. Similar definitions hold for the magnetic and cross correlation functions (note that helicity is a pseudoscalar). Finally, the kinetic and magnetic Reynolds numbers are defined as

$$R_V = U_0 L_0/\nu, \quad R_M = U_0 L_0/\eta,$$

where U_0 and L_0 are the characteristic velocity and length scale, respectively. The integral scale is defined as

$$L_{\rm int} = \frac{\int [E_V(k)/k]dk}{\int E_V(k)dk}.$$

C. Predictions from statistical mechanics

The statistical equilibria in 3D magnetohydrodynamics were derived in Ref. [36]. They are the long-time solutions to a truncated system of Fourier modes, with $k_{\rm min}$ and $k_{\rm max}$ the minimum and maximum wave numbers, respectively; these modes are coupled through the nonlinear ideal MHD equations ($\nu \equiv 0$ and $\eta \equiv 0$) and subject to the conservation of all quadratic invariants. Defining $\alpha \neq 0$, β, and γ as the Lagrange multipliers associated with the E_T, H_M, and H_C invariants, namely, $\alpha E_T + \beta H_M + \gamma H_C$, these equilibria read, assuming that the magnetic helicity is nonzero ($\beta \neq 0$),

$$\begin{aligned} H_M(k) &= -\frac{8\pi\beta}{\alpha^2\Gamma^4}\frac{1}{\mathcal{D}(k)}, \quad H_J(k) = k^2 H_M(k), \\ H_C(k) &= \frac{\gamma\Gamma^2}{2\beta}H_J(k), \quad H_V(k) = \frac{\gamma^2}{4\alpha^2}H_J(k), \end{aligned} \tag{4}$$

$$\begin{aligned} E_M(k) &= -\frac{\alpha\Gamma^2}{\beta}H_J(k) = \frac{8\pi k^2}{\alpha\Gamma^2}\frac{1}{\mathcal{D}(k)}, \\ E_V(k) &= \left(\Gamma^2\mathcal{D}(k) + \frac{\gamma^2}{4\alpha^2}\right)E_M(k) \\ &= \left(1 - \frac{\beta^2}{4\alpha^2\Gamma^2}\frac{1}{k^2}\right)E_M(k), \end{aligned} \tag{5}$$

where $H_J = \int k^2 H_M(k)dk$ is the current helicity and

$$\begin{aligned} &\alpha > 0, \quad \Gamma^2 = 1 - \frac{\gamma^2}{4\alpha^2} > 0, \\ &\mathcal{D}(k) = \left(1 - \frac{\beta^2}{\alpha^2\Gamma^4}\frac{1}{k^2}\right) > 0 \ \forall k \in [k_{\rm min}, k_{\rm max}]. \end{aligned} \tag{6}$$

The invariants H_M and H_C are not definite positive and furthermore H_M does not have the same physical dimension as E_T and H_C and hence β does not have the same physical dimension as α and γ. In order to fulfill realizability conditions (positivity of energy and Schwarz inequalities involving the helicities), necessary relationships between coefficients can be derived, involving $k_{\rm min}$ (see Ref. [36]).

When $\beta \equiv 0$ and thus $H_M(k) \equiv 0$ and $H_J(k) \equiv 0$, one finds that the kinetic helicity is also equal to zero, we have equipartition of energy at all wave numbers with $E_M(k) = E_V(k) = 8\pi k^2/\alpha\Gamma^2$, and $H_C(k) = -4\pi\gamma k^2/\alpha^2\Gamma^2$; thus the relative cross helicity $2H_C(k)/E_V(k)$ is constant in that case. When $\gamma \equiv 0$ and thus $H_C(k) \equiv 0$, the kinetic helicity is also equal to zero and the kinetic energy has its nonhelical expression $E_V(k) = 8\pi k^2/\alpha$; the magnetic energy and helicity can peak at low wave number when β is large enough and the relative magnetic helicity $kH_M(k)/E_M(k) \sim 1/k$, i.e., it is stronger in the largest scales of the flow, a result that persists in the general case ($\beta \neq 0, \gamma \neq 0$).

When considering $H_J(k)$ [instead of $H_M(k)$], note that all Fourier spectra are strictly proportional, with coefficients uniquely determined by initial conditions given the values of the invariants, except for the kinetic energy; also note that one has $E_V(k) \leqslant E_M(k)$ $\forall k$, the equality arising only when there is either no magnetic helicity, or maximal cross correlation, or for $k_{\rm max} \to \infty$. Similarly, the residual helicity defined as

$$H_R(k) = H_V(k) - H_J(k) = -\Gamma^2 H_J(k)$$

is of the sign opposite to that of the current and of the magnetic helicity and $H_R(k)$ becomes equal to zero only for maximal cross correlation ($\Gamma^2 = 0$), except for the trivial nonhelical case of course. The relative helicity $H_R(k)$, integrated over the small scales, is the motor of the nonlinear dynamo problem, i.e., the growth of large-scale magnetic energy because of small-scale helical motions; note that H_R reduces to the kinetic helicity in the kinematic regime when the magnetic field is weak, thus recovering the so-called alpha effect (see Ref. [37] for a recent comprehensive review).

It was shown in Refs. [27,28] that these solutions can be seen as indicators of the long-time behavior of 3D MHD systems left to decay because of a principle of minimization of total energy. Three main regions of parameter space can be seen as attractors to the dynamics: a magnetic helicity dominated region, an alignment (strong H_C) region, and an intermediate region. The relaxation principle is well founded when there is magnetic helicity in the system since dimensionally H_M

weighs the large scales more so than the energy or the cross correlation, but when $H_M \equiv 0$, it is not so clear what happens. It can be shown, using minimum energy principles following Ref. [34], that the resulting fields are $\mathbf{u} = 0$ and $\mathbf{j} \propto \mathbf{b}$ when there is no cross correlation (the constraint is simply that H_M remain constant), whereas in the general case, the solution is a bit more involved [see Eq. (3.13) and those following in Ref. [35]; see also Ref. [28]]. The main purpose of this work is to investigate this long-term dynamics when considering the three initial conditions used in Ref. [15] that have the same quadratic invariants ($E_T = 1/4$, $H_M \equiv 0$, and $H_C \leqslant 4\%$ in relative terms) and thus presumably the same final asymptotic state and yet, at peak of dissipation, show clear differences in their inertial range scaling. We shall also investigate other deterministic flows with either cross helicity or magnetic helicity to see whether they evolve as well towards these attractors.

D. Description of the initial conditions for all the computations

Table I summarizes the main characteristics of the 41 runs discussed in this paper. Further details on the computations are given below, when specifying the initial velocity and magnetic fields. All runs use the Geophysical High-Order Suite for Turbulence code (GHOST) [38] unless otherwise stated in the "Remarks" column; TYGRS stands for a code that implements the fourfold symmetries of the Taylor-Green (TG) flow [39,40] and its extensions to magnetohydrodynamics [15]. Values at $t = T_{100} = 100\tau_{\rm nl}$ of $2H_C/E_T$, H_M/E_T, and E_T, with $\tau_{\rm nl} = L_0/U_0$, are given in the Table; note that $k_{\rm min} = 1$ has been taken as a normalizing factor for the ratio involving magnetic helicity. For all runs $\nu = \eta$ and $E_M = E_V = 0.125$ initially. The groups divided by horizontal lines correspond to different line styles in Figs. 1, 2, and 4. All runs are performed on a grid of 64^3 points with $\nu = 2 \times 10^{-3}$ unless otherwise noted (see the last column); the viscosity is changed inversely to the resolution and three runs are done on grids of 512^3 points, with two in a series (R17** and R25**) with all resolutions from 64^3 to 512^3. Run R17+ is a variant of run R17** on a grid of 512^3 points, with the helical velocity perturbation placed at wave number $k = 1$ instead of $k = 3$. Double and single precision are denoted by D and S, respectively. In the second column I, A, and C refer to the Taylor-Green flows studied in Ref. [15]: They stand for the insulating boundary conditions (I), the alternate insulating conditions (A), and the conducting one (C); by insulating or conducting it is meant that in the box in which the computations are performed, the current is either parallel or normal to the walls. In most cases (except those labeled TYGRS), the symmetries of the Taylor-Green initial conditions are not enforced and can be broken.

Runs in which noise of amplitude 10^{-x} relative to the host flow has been added to both the kinetic and magnetic energies are denoted $+10^{-x}$ in the second column. Furthermore, B wH, B iH, or V&B sH indicates that a weak (1%), intermediate (10%), or small (7%) Beltrami Arnold-Beltrami-Childress (ABC) flow has been added to the velocity or magnetic field initial conditions where the percentages correspond to the relative amount of energy. The run B Hx stands for a modified Taylor-Green velocity and a magnetic field that is a helical Beltrami ABC flow at $k = x$ and the run indicated by V H2, B H2 is the same, but with a 3% addition of ABC added to the velocity. The term OT stands for the Orszag-Tang vortex generalized to three dimensions as the initial condition studied in Ref. [41]. Finally, the last four runs have the velocity of Ref. [41] and a mixture of OT and ABC flow with the specified fractions for the magnetic field. The purpose here is to be able to vary the cross helicity H_C and the magnetic helicity H_M of well-studied configurations in MHD turbulence, at a fixed total energy E_T, the same in all runs; indeed, all computations have equal initial kinetic and magnetic energies, with $E_T = E_V + E_M = 1/4$.

The code GHOST is a general purpose pseudospectral community code with periodic boundary conditions; the code is now parallelized up to ~98 000 processors, using a hybrid (MPI-OpenMP) methodology that becomes advantageous at high resolution [38]. Runs R1b, R5b, and R10b are done using a similar code TYGRS, but in which the fourfold symmetries of the Taylor-Green configuration are enforced at all times [39,40]; TYGRS follows the same parallelization methodology as GHOST. The Taylor-Green velocity is

$$v_x^{\rm TG} = v_0^{\rm TG} \sin k_v x \cos k_v y \cos k_v z,$$
$$v_y^{\rm TG} = -v_0^{\rm TG} \cos k_v x \sin k_v y \cos k_v z, \quad v_z^{\rm TG} = 0$$

and the three different initial conditions for the magnetic field are in that case

$$b_x^I = b_0^I \cos k_m x \sin k_m y \sin k_m z,$$
$$b_y^I = b_0^I \sin k_m x \cos k_m y \sin k_m z,$$
$$b_z^I = -2b_0^I \sin k_m x \sin k_m y \cos k_m z;$$
$$b_x^A = b_0^A \cos k_m x \sin k_m y \sin k_m z,$$
$$b_y^A = -b_0^A \sin k_m x \cos k_m y \sin k_m z, \quad b_z^A = 0$$

and

$$b_x^C = b_0^C \sin k_m x \cos k_m y \cos k_m z,$$
$$b_y^C = b_0^C \cos k_m x \sin k_m y \cos k_m z,$$
$$b_z^C = -2b_0^C \cos k_m x \cos k_m y \sin k_m z.$$

When computations in which these initial fields are perturbed with an added noise, the amplitude of that noise relative to the energy in the Taylor-Green initial condition is indicated in the second column. This noise has randomly generated phases with an energy spectrum of the form

$$N = N_0 \exp\left(-\frac{(\ln k - \ln k_0)^2}{2(\ln \sigma)^2}\right).$$

In all cases the noise is centered around $k_0 = 2$ and has $\sigma = 2$. Noise of this form is added to both the magnetic and kinetic energies and introduces small perturbations in the initial magnetic helicity and cross helicity relative to the total energy depending on the random phases generated and the amplitude of the noise.

We also performed some runs that have significant amounts of helicity since helicity is a main indicator of the behavior of such flows, at least in the ideal regime. Since the Taylor-Green runs have no helicity, different configurations are also studied. The B Hx type is one for which the velocity is a modified Taylor-Green velocity such that $v_x^{\rm TG'} = -v_y^{\rm TG}$, $v_y^{\rm TG'} = -v_x^{\rm TG}$, and $v_z^{\rm TG'} = 0$, centered at wave number 2 or 3, and the magnetic

TABLE I. Initial conditions of the 41 runs, with data at $t = 100\tau_{\rm nl}$ and at the final time T_F. All runs are done on grids of 64^3 points unless otherwise indicated (see the last column), with two series (indicated by two asterisks) with varying Reynolds numbers (and grids) by a factor 8. Values listed for these series are those for the highest resolution (512^3) grid. Three runs are done with the TYGRS code [15,39]. Horizontal lines divide groups with different types of flows and line styles in Figs. 1, 2, and 4. The D and S stand for double and single precision, respectively; I, A, and C are for the TG flows [15]; and $+10^{-x}$ indicates runs with noise of amplitude 10^{-x} relative to the host flows and fields. Runs 15–17 are A flows, double precision, with either weak (w) or intermediate (i) helical perturbations added to the magnetic field (V is also weakly perturbed in the sH cases); H1, H2, or H3 stands for the helical initial conditions at wave number 1, 2, or 3, respectively. The last five runs have **v** as in Ref. [41] and a mixture of OT and ABC with the specified fractions for **b**. See the text for more details.

		Initial values				Values at $T_{100} = 100\tau_{\rm nl}$					Values at $T_F/\tau_{\rm nl}$				
Run	Type	$2H_C/E_T$	H_M/E_T	k_V	k_M	E_M/E_V	$2H_C/E_T$	H_M/E_T	10^4E_T	T_F	E_M/E_V	$2H_C/E_T$	H_M/E_T	10^6E_T	Remarks
R1a	I/D	0.00	0.00	2	2	23.7	0.00	0.00	30.9	500	37.2	0.00	0.00	3.84	
R1b	I/D/T	0.00	0.00	2	2	23.7	0.00	0.00	30.9	500	37.2	0.00	0.00	3.84	TYGRS
R2	I/S	0.00	0.00	2	2	23.5	0.00	0.00	30.9	500	1.91	0.06	0.01	2.26	
R3	$\mathrm{I/D}+10^{-6}$	0.00	0.00	2	2	0.76	−0.01	−0.02	6.18	500	0.99	−0.48	0.08	7.49	
R4	$\mathrm{I/D}+10^{-3}$	0.00	0.00	2	2	0.54	−0.02	0.02	7.83	500	0.58	−0.26	0.08	16.2	
R5a	C/D	0.00	0.00	2	3	0.27	−0.75	0.00	4.80	500	0.84	−1.00	0.00	2.56	
R5b	C/D/T	0.00	0.00	2	3	0.27	−0.75	0.00	4.80	500	0.84	−1.00	0.00	2.56	TYGRS
R6	C/S	0.00	0.00	2	3	0.27	−0.75	0.00	4.80	500	0.84	−1.00	0.00	2.56	
R7	$\mathrm{C/D}+10^{-4}$	0.00	0.00	2	3	0.71	0.05	0.03	2.90	500	0.54	0.21	0.03	6.89	
R8	$\mathrm{C/D}+10^{-3}$	0.00	0.00	2	3	0.75	−0.22	0.01	4.64	500	1.00	−0.71	0.02	16.0	
R9a	$\mathrm{C/D}+10^{-2}$	0.00	0.00	2	3	1.32	0.06	−0.03	4.69	500	1.71	−0.25	−0.11	8.27	
R9b	$\mathrm{C/D}+10^{-2}$	0.00	0.00	2	3	2.33	0.15	−0.12	8.98	100					256^3; $\nu = 6.67 \times 10^{-4}$
R10a	A/D	0.00	0.00	2	3	2.36	0.00	0.00	1.14	500	28.0	0.00	0.00	0.36	
R10b	A/D/T	0.00	0.00	2	3	2.36	0.00	0.00	1.14	500	28.0	0.00	0.00	0.36	TYGRS
R10c	A/D	0.00	0.00	2	3	0.64	0.00	0.00	0.40	1000	0.69	0.00	0.00	1.21×10^{-8}	32^3; $\nu = 4 \times 10^{-3}$
R10d	A/D	0.00	0.00	2	3	4.86	0.00	0.00	1.50	100					128^3; $\nu = 1 \times 10^{-3}$
R11a	A/S	0.00	0.00	2	3	2.36	0.00	0.00	1.14	500	28.0	0.00	0.00	0.36	
R11b	A/S	0.00	0.00	2	3	0.64	0.00	0.00	0.40	1000	0.69	0.00	0.00	1.21×10^{-8}	32^3; $\nu = 4 \times 10^{-3}$
R12	$\mathrm{A/D}+10^{-4}$	0.00	0.00	2	3	1.47	−0.07	0.01	1.50	500	0.65	−0.14	−0.15	3.73	
R13	$\mathrm{A/D}+10^{-3}$	0.00	0.00	2	3	1.45	0.22	−0.01	2.35	500	0.98	0.48	0.06	8.08	
R14	$\mathrm{A/D}+10^{-2}$	−0.01	0.00	2	3	1.44	−0.24	0.08	2.84	500	0.98	−0.45	0.25	7.36	
R15	B wH	0.00	0.00	2	3	0.46	−0.26	−0.02	7.99	500	0.12	−0.16	−0.02	57.7	
R16	B iH	0.00	0.04	2	3	9.30	0.05	0.85	25.8	500	74.81	0.05	0.98	443	
R17**	V&B sH	−0.09	0.02	2, 3	3	8.08	−0.29	0.52	64.9	100					4 runs, 64^3–512^3 grids
R17+	V&B sH+	−0.09	0.00	1, 2	3					50	4.68	−0.12	0.45	8940	512^3; $\nu = 2.5 \times 10^{-4}$ variant
R18	B H1	0.00	0.50	2	1	1428	0.00	1.00	817	100					
R19	B H2	0.00	0.25	2	2	1379	−0.01	0.57	535	100					128^3; $\nu = 1 \times 10^{-3}$
R20	V H2, B H2	0.11	0.25	2	2	177	0.15	0.57	282	500	155	0.13	0.99	1018	
R21a	B H3	0.00	0.17	3	3	20.5	0.00	0.85	316	150	60.2	0.00	0.94	2.71×10^5	192^3; $\nu = 6.67 \times 10^{-4}$
R21b	B H3	0.00	0.17	3	3	17.4	0.00	0.80	363	150	49.7	0.00	0.92	3.03×10^5	256^3; $\nu = 5 \times 10^{-4}$
R22	OT	0.41	0.00	1	1, 2	1.00	0.99	0.00	21.0	250	0.99	1.00	0.00	337	
R23a	0.99OT + 0.01H1	0.41	0.00	1	1, 2	0.98	0.99	0.12	19.7	150	1.02	1.00	0.13	957	
R23b	0.99OT + 0.01H1	0.41	0.00	1	1, 2	1.05	0.99	0.10	62.4	150	1.04	1.00	0.12	4032	256^3; $\nu = 5 \times 10^{-4}$
R24	0.95OT + 0.05H1	0.41	0.02	1	1, 2	1.95	0.92	0.51	32.0	150	2.03	0.92	0.57	1863	
R25**	0.5OT + 0.5H1	0.40	0.31	1	1, 2					50	10.89	0.53	0.89	8.11×10^4	4 runs, 64^3–512^3 grids

field is a Beltrami ABC flow centered at wave number $k_m = x$ with x equal to either 1, 2, or 3; the ABC magnetic field is

$$b_x^{\rm ABC} = b_0^{\rm ABC}[B\cos(k_m y) + C\sin(k_m z)],$$
$$b_y^{\rm ABC} = b_0^{\rm ABC}[C\cos(k_m z) + A\sin(k_m x)],$$
$$b_z^{\rm ABC} = b_0^{\rm ABC}[A\cos(k_m x) + B\sin(k_m y)].$$

The OT configuration is that of the generalization of the Orszag-Tang vortex to three dimensions, as studied in Ref. [41], with the velocity and magnetic fields defined as

$$v_x^{\rm OT} = -2v_0^{\rm OT}\sin k_v y, \quad v_y^{\rm OT} = 2v_0^{\rm OT}\sin k_v x, \quad v_z^{\rm OT} = 0$$

and

$$b_x^{\rm OT} = b_0^{\rm OT}[-2a\sin 2k_m y + a\sin k_m z],$$
$$b_y^{\rm OT} = b_0^{\rm OT}[2a\sin k_m x + a\sin k_m z],$$
$$b_z^{\rm OT} = b_0^{\rm OT}[a\sin k_m x + a\sin k_m y].$$

The parameter a allows one to modify the cross correlation between the two fields; the choice $a = 0.8$ gives a relative correlation of 0.41.

Finally, initial conditions that are mixtures of the above types are also studied. Runs R15 and R16 have the Taylor-Green velocity and perturb the Taylor-Green magnetic field initial condition with an A configuration, with an ABC Beltrami field such that

$$b_x^{\rm A+ABC} = b_0^{A+\rm ABC}\{(\xi_1\cos k_{m1}x\,\sin k_{m1}y\,\sin k_{m1}z + \xi_2[B\cos(k_{m2}y) + C\sin(k_{m2}z)]\},$$
$$b_y^{\rm A+ABC} = b_0^{A+\rm ABC}\{-\xi_1\sin k_{m1}x\,\cos k_{m1}y\,\sin k_{m1}z + \xi_2[A\sin(k_{m2}x) + C\cos(k_{m2}z)]\},$$
$$b_z^{\rm A+ABC} = b_0^{A+\rm ABC}\xi_2[A\cos(k_{m2}x) + B\sin(k_{m2}y)].$$

The parameters ξ_1 and ξ_2 set the relative fractions of the Taylor-Green and ABC portions of the initial condition. Run R15 has $\xi_1 = 0.99$ and $\xi_2 = 0.01$ and run R16 has $\xi_1 = 0.9$ and $\xi_2 = 0.1$. Both of these flows have k_{m1} and k_{m2} such that both portions of the initial condition are at $k = 3$. Initial conditions such as these allow for a perturbation in the magnetic helicity without significantly perturbing the cross helicity. The series of runs labeled R17** use the above combined magnetic field, but also have a velocity that combines the Taylor-Green and ABC flows in a similar fashion:

$$v_x^{\rm TG+ABC} = v_0^{\rm TG+ABC}\{\xi_1\sin k_{v1}x\,\cos k_{v1}y\,\cos k_{v1}z + \xi_2[B\cos(k_{v2}y) + C\sin(k_{v2}z)]\},$$
$$v_y^{\rm TG+ABC} = v_0^{\rm TG+ABC}\{-\xi_1\cos k_{v1}x\,\sin k_{v1}y\,\cos k_{v1}z + \xi_2[A\sin(k_{v2}x) + C\cos(k_{v2}z)]\},$$
$$v_z^{\rm TG+ABC} = v_0^{\rm TG+ABC}\xi_2[A\cos(k_{v2}x) + B\sin(k_{v2}y)].$$

In the case of the R17 runs, both the magnetic field and velocity initial conditions have $\xi_1 = 0.93$ and $\xi_2 = 0.07$. The magnetic field is such that both portions of the initial condition are at $k = 3$, but the velocity has the Taylor-Green portion of the flow at $k = 2$ and the ABC portion at $k = 3$ initially. This allows for a perturbation in both the magnetic helicity and cross helicity. Run R17+ is the same, but with the ABC portion of the velocity at $k = 1$. Run R20 involves a velocity that is a combination of the modified Taylor-Green velocity and a Beltrami ABC flow such that

$$v_x^{\rm TG'+ABC} = v_0^{\rm TG'+ABC}\{\xi_1\cos k_{v1}x\,\sin k_{v1}y\,\cos k_{v1}z + \xi_2[B\cos(k_{v2}y) + C\sin(k_{v2}z)]\},$$
$$v_y^{\rm TG'+ABC} = v_0^{\rm TG'+ABC}\{-\xi_1\sin k_{v1}x\,\cos k_{v1}y\,\cos k_{v1}z + \xi_2[A\sin(k_{v2}x) + C\cos(k_{v2}z)]\},$$
$$v_z^{\rm TG'+ABC} = v_0^{\rm TG'+ABC}\xi_2[A\cos(k_{v2}x) + B\sin(k_{v2}y)].$$

In run R20, $\xi_1 = 0.97$, $\xi_2 = 0.03$, and k_{v1} and k_{v2} are set such that both the Taylor-Green and ABC subsets of the initial flow are at $k = 2$. When combined with an ABC magnetic field, this results in the addition of cross correlation between the velocity and magnetic fields of 0.11 relative to the total energy.

The type ξ_1 OT + ξ_2 H1 is an initial condition for the velocity that is the OT vortex and combines the OT and ABC magnetic fields such that

$$b_x^{\rm OT+ABC} = b_0^{\rm OT+ABC}\{\xi_1[-2a\sin 2k_{m1}y + a\sin k_{m1}z] + \xi_2[B\cos(k_{m2}y) + C\sin(k_{m2}z)]\},$$
$$b_y^{\rm OT+ABC} = b_0^{\rm OT+ABC}\{\xi_1[2a\sin k_{m1}x + a\sin k_{m1}z] + \xi_2[A\sin(k_{m2}x) + C\cos(k_{m2}z)]\},$$
$$b_z^{\rm OT+ABC} = b_0^{\rm OT+ABC}\{\xi_1[a\sin k_{m1}x + a\sin k_{m1}y] + \xi_2[A\cos(k_{m2}x) + B\sin(k_{m2}y)]\},$$

where ξ_1 and ξ_2 set the relative fractions of OT and ABC, respectively. Each of the flows of this type is such that $k_{m1} = k_{m2} = 1$. Some runs were performed for more than $1000\tau_{\rm nl}$, where $\tau_{\rm nl} = L_0/U_0$ is the turnover time, and the maximum number of modes in the largest runs on grids of 512^3 points is in excess of 10^6.

E. Global properties for all the runs

We show in Fig. 1 the temporal evolution of the Reynolds number [Fig. 1(a)] and of the ratio of magnetic to kinetic energy [Fig. 1(b)] for roughly half the runs. The color table and symbols for runs are also given in Fig. 1. Since the runs are performed at relatively modest Reynolds numbers and numerical resolutions but for long times, the Reynolds numbers eventually enter a regime of exponential decay where nonlinearities are weak. The burst of energy for run R20 at $t \sim 250$ is associated with the end of a plateau in the ratio E_M/E_V and with a weak Lamb vector $\mathcal{L} = \mathbf{v}\times\boldsymbol{\omega}$ (see Fig. 4 below). Examining the energy ratio, it is clear that two main regime types develop in these runs: One is close to equipartition, with a tendency to have an excess in magnetic energy as predicted by the statistical ensembles, and one is where the magnetic energy wins all and is presumably under the influence of a strong relative magnetic helicity and an accumulation of H_M at the gravest mode of the computation. The run done on a grid of 32^3 points has its Reynolds number getting too low and as a result behaves considerably differently from the other Taylor-Green A flow runs on grids of 64^3 and 128^3 points. Of course $\mathbf{v} = 0$ is a possible solution of the MHD equations; this corresponds to the hydrodynamic attractor, which can also be fluid in the forced case when the magnetic Reynolds number is too low. Also note that run R15, which is the Taylor-Green A flow perturbed by 1% ABC magnetic field, moves towards a kinetically dominated state;

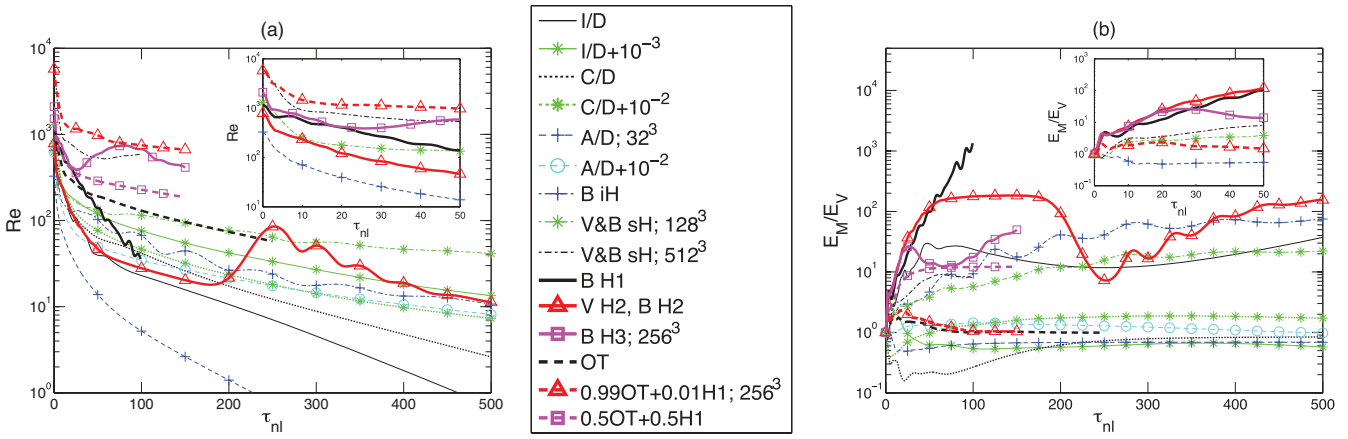

FIG. 1. (Color online) (a) Evolution of the Reynolds number defined as $\mathrm{Re} \equiv v_{\mathrm{rms}} L_{\mathrm{int}}/\nu$, where L_{int} is the integral scale (see the text) as a function of time for roughly half of the flows from Table I. The plot is in linear-logarithmic coordinates and time is measured in units of turnover time for each configuration. The inset shows a blowup of the results for early times for a subset of plotted runs. Each run is indicated by symbols (and colors online) that are given in the center. (b) Magnetic to kinetic energy ratio for the same runs in linear-logarithmic coordinates. Many runs gather around quasiequipartition either above or below, but for some runs, mostly those in which the relative amount of magnetic helicity grows significantly (such as runs R16–R21b), this ratio becomes substantially larger than unity.

by the end of the run, this flow has kinetic energy dominating over magnetic energy by approximately a factor of 10 in the gravest mode.

II. ROLE OF ACCURACY AND SYMMETRIES

The ensemble of runs analyzed in this paper is shown in Fig. 2 in a plane introduced in Refs. [27,28]; it delineates, in terms of the total energy, the relative importance of the two helical invariants. A peculiar feature of the I and A Taylor-Green runs is that, unless perturbed, they stay where they started, even though in these runs the symmetries are not imposed at all times. This may be related to the fact that it can be shown that, in the context of the fluid equations, symmetries are preserved by the dynamical evolution, a result that one may be able to extend to the MHD case [42]. Unperturbed, these two flows do not evolve in parameter space at these low Reynolds numbers. In the presence of perturbations, they do cover parameter space and evolve towards configurations with either strong H_M (and thus high ratio E_M/E_V, as in the case of runs R16 and R17**) or strong H_C with near equipartition of kinetic and magnetic energies. Note that, in single precision and for long times, the I flow is perturbed by the accumulated roundoff errors and it evolves toward another attractor, as shown in Fig. 3: Whereas the accurate computation that maintains all symmetries evolves toward presumably a magnetically dominated Taylor state, the errors introduced by insufficient precision lead to a quasiequipartition of energy. This same behavior, where the single-precision computation evolves towards a different attractor after sufficiently long times, is not evident in either the A or C Taylor-Green flows; however, similar effects are observed when random noise is explicitly added to these initial conditions.

The C flow also exhibits unique behavior as compared to the I and A flows in that, over the course of the computation, the accurate double-precision run does not remain at the origin of the plane and instead moves to a state with $2H_C/E_T = -1$ and $H_M/E_T = 0$. As a result, the C flow without perturbations reaches an equipartitioned state, as opposed to a magnetically dominated state.

We have also performed a more controlled and specific perturbation of the Taylor-Green symmetries by adding a fraction of a Beltrami ABC flow to the magnetic field and/or velocity of the Taylor-Green initial condition in the A configuration, i.e., by perturbing the flow explicitly with nonzero helicity (runs R15–R17+ and R18–R21b). By varying the amount of helical ABC flow relative to nonhelical Taylor-Green flow in the magnetic field, the value of H_M/E_T can be adjusted in a controlled manner at $t = 0$. By also adding a fraction of ABC flow to the velocity, a set amount of $2H_C/E_T$ can additionally be introduced to the flow. With larger perturbations to the magnetic helicity and cross helicity, such as in runs R16 and R17**, the symmetries are clearly broken and the runs reach the boundaries of the parameter space as predicted by the minimum energy principle (see Fig. 2). Note that run R17d, which is performed on a grid of 512^3 points, is only run for $100\tau_{\mathrm{nl}}$. If this run were continued to longer times, as the other three R17** runs are, this run would likely reach the boundary. In the case of run R16, only the magnetic field initial condition is perturbed with 10% ABC flow and the flow achieves a magnetically dominated state with nearly maximal H_M/E_T. The four R17** runs, which all have 7% ABC flow in both the velocity and magnetic field initial conditions, but are performed at different Reynolds numbers, evolve to a state on the boundary with both nonzero H_M/E_T and $2H_C/E_T$ when given enough time. Note that although the four runs have the same initial conditions, they have taken different paths through the parameter space with differing Reynolds number due to the effect of small perturbations.

III. INTERPLAY BETWEEN HELICAL INVARIANTS

A. Magnetic helicity relative growth

According to the equations written in Sec. I C, the helical invariants play a central role in the evolution of MHD

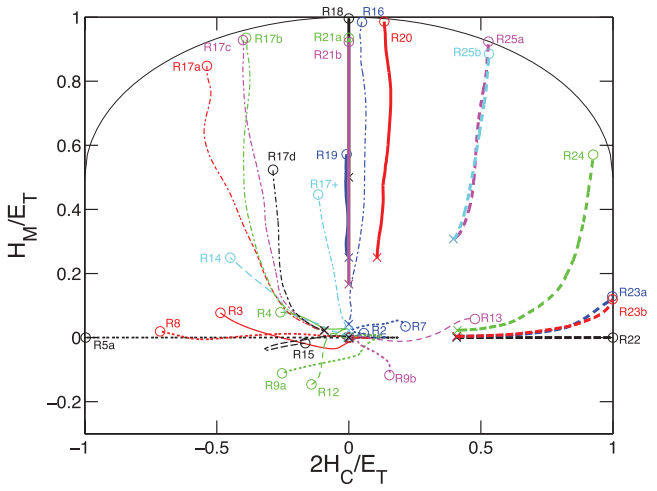

FIG. 2. (Color online) Trajectories taken through the $(2H_C/E_T, H_M/E_T)$ parameter space for the runs in Table I. The start positions for each run are marked with $\times$ and the positions at the final time of the run are marked with $\circ$. Each curve is labeled with the run number from Table I near the end point. Three runs (R5a, R5b, and R6) follow the black dotted line, which goes from the origin to the point $(-1,0)$, and eight runs (R1a, R1b, R10a–R10d, R11a, and R11b) remain at the origin of the parameter space; note that this origin is unstable and when symmetries are broken by perturbations, the resulting trajectories can go in any direction depending on the phases of the perturbation. The two series (R17** and R25**) have the asterisks replaced with letters that progress from a to d for increasing resolutions to mark the individual runs. Only the 64^3 and 512^3 runs are shown from R25** because all resolutions followed nearly identical trajectories. The energy minimization principle predicts that flows will move towards the boundaries of this space; that is, $2H_C/E_T = \pm 1$ when the end value of $H_M/E_T < 0.5$ and on the marked ellipsoidal curve bounding the upper portion of the plot when the end value of $H_M/E_T \geqslant 0.5$. The parameter space is symmetric for negative values of H_M/E_T.

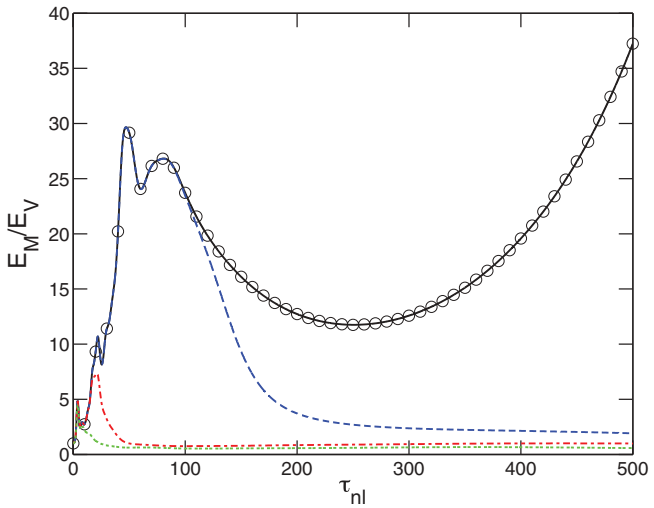

FIG. 3. (Color online) Comparison for the magnetic to kinetic energy ratio for the Taylor-Green I flow between two codes, one implementing symmetries (run R1b, black circles), the other one not (run R1a, black solid line), both in double precision, together with another run using single precision (run R2, blue dashed line). The double precision in GHOST is sufficient to maintain the symmetries up to $T = 500$, in units of turnover times. Note the excellent agreement between the three computations performed on a grid of 64^3 points up to $T \sim 100\tau_{\rm nl}$, the time after which the single-precision run departs from the others and evolves towards quasiequipartition (at the final time $E_M/E_V \sim 2$, as often observed in the solar wind [4]). The red dash-dotted line and the green dotted line are the Taylor-Green I flow with added random noise of relative amplitudes 10^{-6} (run R3) and 10^{-3} (run R4), respectively. Note that added noise behaves similarly to the single-precision computation, but departs from the other runs and goes towards quasiequipartition at earlier times.

turbulence. Since the Taylor-Green flows have no helicity, we now examine a set of evolutions for several helical configurations that have been studied in the literature, namely, the ABC (Beltrami) flows, the Orszag-Tang vortex, and some perturbations of such flows (see Sec. I D and Table I for definitions).

The Orszag-Tang vortex, without magnetic helicity, becomes highly correlated, but with the inclusion of some magnetic helicity it evolves toward states that, as H_M/E_T increases, are more and more magnetically dominated. With very small additions of magnetic helicity (runs R23a and R23b), H_M/E_T grows to modest values at which $2H_C/E_T$ can still obtain a value of one and the flow has equipartition between kinetic and magnetic energies. However, with even a slightly larger addition of H_M (see runs R24 and R25** of Table I), the growth of H_M/E_T begins to dominate and the flow moves towards more magnetically dominated states. Similarly, unperturbed ABC flows, with strong H_M, remain uncorrelated if initially so; however, when perturbing them by adding some correlation between the velocity and the magnetic field, as in run R20, they follow similar evolutions but stay away from the singularity that occurs at maximum $H_M/E_T, H_C \equiv 0$.

B. Vector alignment in MHD turbulence

The relative alignment of dynamical fields [see Eq. (3) for definitions] is shown in Fig. 4 for many runs, using the same line (color) encoding as in Fig. 1. Many runs reach an Alfvén state ($\sigma_C \sim \pm 1$), some more slowly, and a few stay at low values: It has been known for a long time that the correlation between the velocity and the magnetic field grows with time (see, e.g., Ref. [35]).

Magnetic helicity seems more discriminating insofar as the long-time behavior of the runs: Either $k_{\rm min} H_M/E_T$ remains rather low or it approaches its maximal value. The runs that approach near maximal values of H_M/E_T are those in which a sufficient amount of magnetic helicity is present in the initial condition. In Fig. 2, as well as in Fig. 4, it can be seen that all the runs that attain large values of H_M/E_T have at least slightly larger initial values of magnetic helicity than those that remain near zero. In contrast, the normalized kinetic helicity shows a more varied set of behaviors, with sometimes strong fluctuations between aligned and perpendicular fields, as for run R20 [thick solid red line (triangles)], which evolves towards strong magnetic helicity (see the map in Fig. 2). Note that run R25 [thick dashed purple line (squares)] is likely to evolve in a similar manner. This analysis suggests that one ought to look in more detail at the alignment properties of the

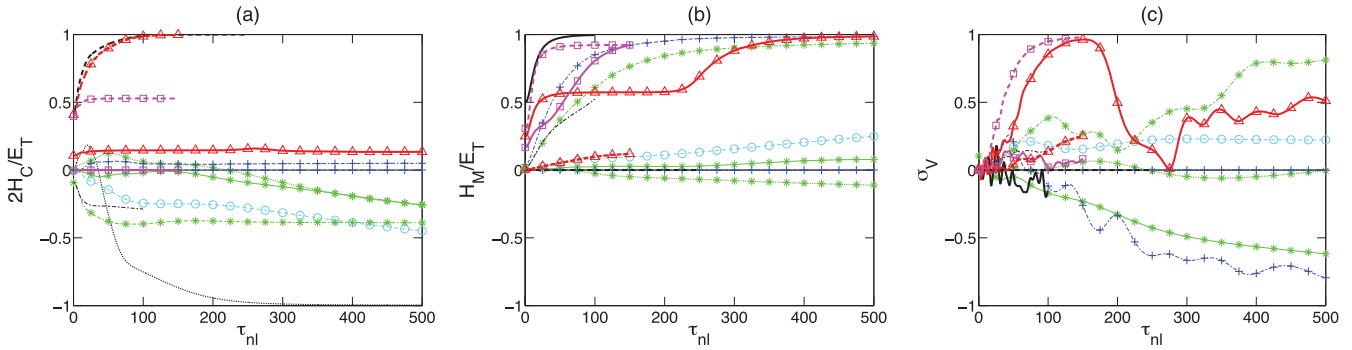

FIG. 4. (Color online) Temporal evolution of helicity in relative terms for the runs in Fig. 1, with (a) H_C/E_T, (b) $k_{\min}H_M/E_T$, and (c) σ_V [see definition in Eq. (3)]. The symbols and color scheme are the same as in Fig. 1. Note the clear distinction between the runs for the two invariant quantities (staying at values close to either zero or their extrema) and the more varied evolution for σ_V, although its evolution is also influenced by magnetic helicity [see Eq. (4)].

various fields by examining probability distribution functions (PDFs) of the angle between various vectors.

The buildup of pointwise correlations between vector fields in a turbulent flow (velocity and vorticity in the fluid case, velocity and magnetic induction in the MHD case) in a few turnover times is a dynamical consequence of the primitive equations and is linked to the alignment of vorticity with either pressure gradients or shear [43]; it occurs both in DNS of MHD flows and perhaps more importantly in the solar wind (as could be shown in Ref. [43] using 30 years of Omni data). These points were further studied in detail in Ref. [33] with 3D computations; the strongest alignment property was found to be between induction and current (corresponding to a weakening of the Lorentz force) and with, for all vectors, a strong enhancement over their Gaussian values.

In this context, we show in Fig. 5 alignment probability distribution functions for several variables for several flows (see the caption), after ten turnover times: Row (u) is for velocity and magnetic field (concentrating on the cross helicity); row (um) examines the magnetic potential and magnetic field, i.e., considering magnetic helicity; row (lm) looks at the Lorentz force, i.e., the degree of alignment between induction and current; and row (l) considers the Lamb vector, i.e., the degree of alignment between the velocity and the vorticity. At $t = 0$, all undisturbed flows have a strong central peak corresponding to orthogonality of vectors (either $\mathbf{A} \perp \mathbf{b}$ or $\mathbf{v} \perp \mathbf{b}$) and thus strong nonlinearities, except for the OT case [column (d)], for which σ_M peaks symmetrically at values slightly greater and slightly less than zero and σ_C indicates that there is a significant fraction of highly aligned velocity and magnetic field vectors.

These PDFs confirm the results illustrated in Fig. 2 in showing an evolution towards either alignment of the velocity and the magnetic field, or of the magnetic field and the potential, once the flows are perturbed, the more so the larger the perturbation and the more so the smaller the scale (as when contrasting $[\mathbf{A},\mathbf{b}]$ and $[\mathbf{j},\mathbf{b}]$), as can be observed for all flows. The I flows [column (a)] are in fact the harder to perturb insofar as alignment does not really develop and one only observes a widening of the PDFs around zero, i.e., a distribution of angles that remains nevertheless close to $\pi/2$, with the magnetic field and current developing alignment, particularly so for the stronger the perturbation. For the C flow family of runs [column (b)], a perturbation at the level of 10^{-x} simply widens the distribution of angles (blue dashed curve), but increasing this perturbation leads to a totally different behavior and a flat distribution for magnetic helicity, the perturbations being less significant for cross helicity in the sense that the PDF is changed, but the overall distribution (its shape) is similar in all cases.

Concerning the A configuration [column (c)], as the flows are more perturbed from their highly symmetric initial conditions, the fields become more aligned, with an almost equal distribution for $\mathbf{v}$ and $\mathbf{b}$ ($\sigma_C \sim \pm 1$), whereas a clear alignment develops for $\mathbf{a}$ and $\mathbf{b}$ [$\sigma_M \sim 1$ for run R14 with the strongest perturbation, with a similar strong (positive) alignment between the current and magnetic field]. Finally, the Orszag-Tang flow [column (d)] starts from a different configuration of vectors and its evolution as it is more perturbed is not so dramatically different (except for the green dash-dotted line, which corresponds to an initial condition with a 50% OT–50% ABC mixture).

In contrast, the relative kinetic helicity (corresponding to alignment of velocity and vorticity) does not seem to follow such a clear-cut organization unless magnetic helicity is strong and kinetic helicity follows H_M and grows in relative terms, under the influence presumably of Alfvén waves due to the large-scale magnetic field, as predicted in Ref. [44]. However, the A and C flows show less weakening of the advection term than for the other two fields, with rather flat PDFs for $[\mathbf{u},\omega]$. The growth of $\mathbf{v} - \omega$ or $\mathbf{v} - \mathbf{b}$ alignment is a dynamical property of the Navier-Stokes or MHD equations, corresponding to the mutual interactions of shear and vorticity or shear and magnetic field [43]; in fact, such alignments properties have been found between all relevant fields, to different degrees [33]. Alignment (and subsequent weakening of nonlinear interactions) is shared by the moderate Reynolds number computations performed here and for long times as well.

C. Is there a dynamically significant ratio in MHD turbulence?

We finally examine the relative role of the velocity and the magnetic field, in terms of energy distribution and time scales, for the runs performed at the highest Reynolds number and

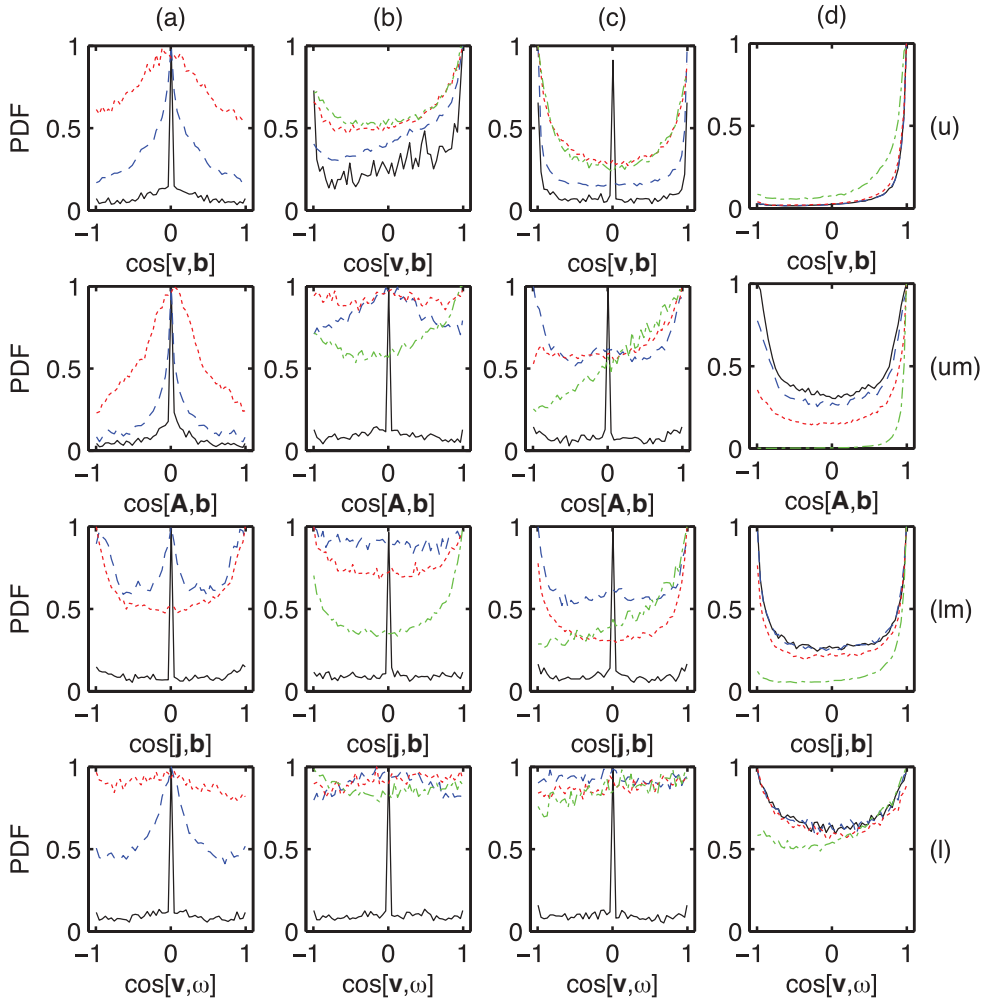

FIG. 5. (Color online) Probability distribution functions at $T = 10\tau_{\rm nl}$ of the cosine of the angle between the velocity and magnetic field **b** [row (u)], the magnetic potential and the magnetic field (row (um)), and **b** and current density [row (lm)]. Finally, row (l) gives the alignment between velocity and vorticity, i.e., examining the Lamb vector. All PDFs are normalized to their maximum value. Column (a) I flow runs R1a (black solid line), R3 (blue dashed line), and R4 (red dotted line); column (b) C flow runs R5a (black solid line), R7 (blue dashed line), R8 (red dotted line), and R9a (green dash-dotted line); column (c) A flow runs R10a (black solid line), R12 (blue dashed line), R14 (red dotted line), and R16 (green dash-dotted line); column (d) OT flow runs R22 (black solid line), R23a (blue dashed line), R24 (red dotted line), and R25 (green dash-dotted line). See Table I for the nomenclature of the runs.

thus with the largest extent of the inertial range (and numerical grid resolution). In order to do so, we look at the behavior in the inertial range around the peak of dissipation, when the turbulence is developed and the Reynolds number has not decreased substantially yet, of the ratio of magnetic to kinetic energy $r_E(k) = E_M(k)/E_V(k)$ and of the eddy turn-over time to the Alfvén time $r_\tau(k) = \tau_{\rm nl}(k)/\tau_A(k)$, the latter being built on the magnetic field in the gravest mode.

The ratio of time scales behaves as expected when evaluating the turnover time on the energy spectrum variation with wave number. This can be seen in Fig. 6: For all flows, $r_\tau(k)$ increases with decreasing scale because of the way these two characteristic times change with scale, i.e., $1/k$ for τ_A and $[k^3 E_V(k)]^{-1/2}$ for the eddy turnover time. In contrast, and again for all flows, the energy ratio is constant and of order unity (but systematically slightly above in fact, as also regularly observed often in the solar wind), except in the largest scale in which it is dominated by initial conditions and the reinforcement of magnetic energy in the largest scale in all the runs dominated by an evolution towards the top of the map displayed in Fig. 2 and corresponding to cases with strong magnetic helicity. We also display for completion the kinetic, magnetic, and total energy spectra for the R17** flow in Fig. 6(c); of course, the resolution for these runs prevents us from distinguishing whether a Kolmogorov or an IK scaling is favored here. Note that at later times of the order of three times the peak of dissipation, this result still holds but with, in all cases displayed here, an increase in E_M/E_V at the largest excited scales, by a factor of 2–40 (not shown). All other runs of this study behaved similarly, as long as the Reynolds number is sufficiently high for turbulent mixing to take place.

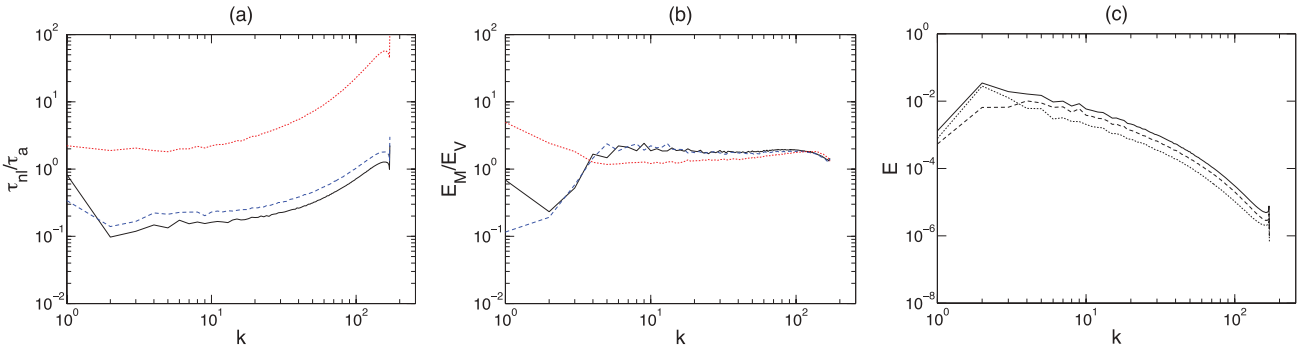

FIG. 6. (Color online) (a) Nonlinear to Alfvén time ratio and (b) magnetic to kinetic ratio, as functions of wave number at the peak of dissipation for the following computations performed on grids of 512^3 points (see Table I for the nomenclature): run R17** [A flow with 7% ABC flow (black solid line)], run R17+ [variant of A flow with 7% ABC flow (blue dashed line)], and run R25 [50% OT flow and 50% ABC flow (red dotted line)]. Note the constancy of quasiequipartition of energy throughout the inertial range, to be contrasted with the increase in the ratio of characteristic time scales in that same range. (c) Spectra (kinetic, magnetic, and total with dotted, dashed, and solid lines respectively) for R17** on the 512^3 grid.

IV. CONCLUSION

In this paper we tackled the problem of long-time properties of turbulent flows in magnetohydrodynamics at unit magnetic Prandtl number, using direct numerical simulations with grids of up to 512^3 points. This was done for flows and magnetic fields with periodic boundary conditions appropriate for homogeneous turbulence. We chose a variety of flows and examined the effect of perturbing the initial conditions with different levels of random noise, as well as modifying the ideal invariants in the fluid at constant total energy, namely, the magnetic helicity that quantifies the degree of knottedness of the flow, and the correlation between the velocity and magnetic field. We show that, independently of the Reynolds number (up to a maximum Reynolds number of approximately 1.2×10^4), flows evolve to a state based on basic physical principles, namely, using the statistical equilibria of a truncated number of modes with the given chosen invariants, combined with an energy minimization principle [27].

Specifically, we showed that the Taylor-Green configurations, studied in Ref. [15] for their energetic properties, depart from their strong symmetries given a sufficiently strong perturbation, as can be encountered in high Reynolds number flows. They then evolve toward different characteristic behaviors as to the amount of magnetic and cross helicity they support (in the H_M-H_C plane; see the temporal trajectories of runs in Fig. 2). These can depend on the perturbation (whether it has cross correlation or magnetic helicity), leading the flows to different end states in particular. It is not clear, however, if, when studying these flows at substantially higher Reynolds numbers, as was done in Ref. [15] for the Taylor-Green flows in magnetohydrodynamics but, contrary to Ref. [15], not imposing the symmetries at all time, one will still have three different scaling laws for the total energy spectra for these three configurations. We also confirm that statistical mechanics, with an energy minimization principle, is an excellent predictor for the behavior of turbulent flows, as argued in Ref. [27] and studied at moderate resolutions in Ref. [28]. The conclusion on the validity of statistical mechanics for dissipative turbulent flows in magnetohydrodynamics is reached using a parametric study for a variety of initial conditions and with grids of up to 512^3 points and Reynolds numbers of up to 12 000 (values taken at $t = 0$), a substantial improvement over previous studies.

How generic are the flows studied in this paper? One could think in terms of random initial conditions, as initially done in Refs. [27,28]; the view here is that noise is generic in experimental or geophysical flows and the question is what emerges over time through the nonlinear interactions in the general case. Turbulence would be a boring subject if it was Gaussian; in fact, phase relations play an important role in the structuring of turbulent flows, with a wealth of well-defined structures, be it vortex filaments for fluids or vortex and current sheets in magnetohydrodynamics; such sheets eventually roll up at sufficiently high Reynolds number, as observed in high-resolution DNS of MHD flows [19] and as observed as well in the solar wind [13]. The instabilities of such structures eventually lead to energy dissipation, as measured recently in a series of studies (see, e.g., Refs. [45–49]).

In contrast, the initial conditions of a turbulent event, in the solar wind environment or in the interstellar medium, two cases where MHD turbulence is known to play a role, may well come from an instability when, for some reason, the fluid goes over threshold. One can think, for example, of a stably stratified medium such as in an atmosphere (or in the oceans of planet Earth) in which, through nonlinear couplings of weak waves, overturning and Kelvin-Helmoltz instability take place, leading, for example, to enhanced diffusion [50]. These instabilities near threshold may well be represented by a few large-scale modes, which may result in different alignment properties (in other words, different σ's). Finally, one could point out that, in principle, universality (within a given class) holds whatever the initial conditions, classes that can be described by the ideal invariants and likely by the initial ratio of kinetic to magnetic energy as well [15].

Quasiequipartition between the kinetic and magnetic energies is expected, on the basis of mixing of complex systems with a large number of degrees of freedom, although, as shown

in Ref. [36], magnetic helicity, alone or in the presence of cross helicity, may well prevent this from happening. What we have shown in this paper is that, in some cases with strong phase relationships such that the nonlinear terms are weakened considerably through alignment of the relevant fields (vorticity, velocity, magnetic field, and magnetic current), other solutions are reachable with quite different properties. This is a bit akin to a potential flow in hydrodynamics: When the vorticity is identically zero, this is an exact solution of the Navier-Stokes equations, although an unstable one, and vorticity, like a seed magnetic field, grows over time. The reason why these solutions do not destabilize in a Lyapounov time, which can be close to an eddy turnover time, is probably due to the fact that symmetries are very strong properties of flows that are preserved by the dynamical evolution [42,51]. This, as well as other open questions, is a topic for future work.

ACKNOWLEDGMENTS

Help in startup runs from Duane Rosenberg is gratefully acknowledged. The National Center for Atmospheric Research, where the computations were performed, is sponsored by the National Science Foundation. This material is based upon work supported by the National Science Foundation Graduate Research Fellowship under Grant No. DGE 1144083 for J.E.S. Finally, M.-E.B. acknowledges a Computational and Information Systems Laboratory fund allocation.

[1] M. Opher *et al.*, Nature (London) **462**, 1036 (2009).
[2] J. Saur, A. Pouquet, and W. H. Matthaeus, Geophys. Res. Lett. **30**, 1686 (2003).
[3] L. C. Ray *et al.*, J. Geophys. Res. **117**, A01205 (2012).
[4] W. H. Matthaeus and M. Goldstein, J. Geophys. Res. **87**, 6011 (1982).
[5] R. Bruno and V. Carbone, http://www.livingreviews.org/lrsp-2005-4.
[6] E. Falgarone, J. Pety, and P. Hily Blant, Astron. Astrophys. **507**, 355 (2009).
[7] M. Opher *et al.*, Astrophys. J. **734**, 71 (2011).
[8] F. Sahraoui, M. L. Goldstein, G. Belmont, P. Canu, and L. Rezeau, Phys. Rev. Lett. **105**, 131101 (2010).
[9] S. Galtier *et al.*, J. Plasma Phys. **63**, 447 (2000).
[10] S. Galtier *et al.*, Astrophys. J. Lett. **564**, L49 (2002).
[11] S. Galtier, *Wave Turbulence*, edited by V. Shrira and S. Nazarenko (World Scientific, Singapore, 2011).
[12] S. L. G. Hess, D. M. Malaspina, and R. E. Ergun, J. Geophys. Res. **116**, A07104 (2011).
[13] H. Hasegawa *et al.*, Nature (London) **430**, 755 (2004).
[14] S. Eriksson, *et al.* J. Geophys. Res. **114**, A00C17 (2009).
[15] E. Lee, M. E. Brachet, A Pouquet, P. D. Mininni, and D. Rosenberg, Phys. Rev. E **81**, 016318 (2010).
[16] G. Krstulovic, M. E. Brachet, and A. Pouquet (unpublished).
[17] A. Alexakis, P. D. Mininni, and A. Pouquet, Phys. Rev. E **72**, 046301 (2005).
[18] P. D. Mininni, A. Alexakis, and A. Pouquet, Phys. Rev. E **72**, 046302 (2005).
[19] A. Pouquet *et al.*, Geophys. Astrophys. Fluid Dyn. **104**, 115 (2010).
[20] T. Gomez, H. Politano, and A. Pouquet, Phys. Fluids **11**, 2298 (1999).
[21] P. D. Mininni, A. Alexakis, and A. Pouquet, Phys. Rev. E **74**, 016303 (2006).
[22] H. Mouri, A. Hori, and M. Takaoka, Phys. Fluids **21**, 065107 (2009).
[23] K. R. Sreenivasan and G. Stolovitzky, Phys. Rev. Lett. **77**, 2218 (1996).
[24] J. A. Domaradzki and R. Rogallo, Phys. Fluids A **2**, 413 (1990).
[25] J. Shebalin, Plasma Phys. **16**, 072301 (2009).
[26] P. D. Mininni, P. Dmitruk, W. H. Matthaeus, and A. Pouquet, Phys. Rev. E **83**, 016309 (2011).
[27] T. Stribling and W. H. Matthaeus, Phys. Fluids B **2**, 1979 (1990).
[28] T. Stribling and W. H. Matthaeus, Phys. Fluids B **3**, 1848 (1991).
[29] R. H. Kraichnan and R. Panda, Phys. Fluids **31**, 2395 (1988).
[30] R. M. Kerr, Phys. Rev. Lett. **59**, 783 (1987).
[31] M. Meneguzzi *et al.*, J. Comput. Phys. **123**, 32 (1996).
[32] W. H. Matthaeus and D. Montgomery, Ann. N.Y. Acad. Sci. **357**, 203 (1980).
[33] S. Servidio, W. H. Matthaeus, and P. Dmitruk, Phys. Rev. Lett. **100**, 095005 (2008).
[34] L. Woltjer, Proc. Natl. Acad. Sci. USA **44**, 833 (1958).
[35] A. Pouquet, in *Magnetohydrodynamic Turbulence*, edited by J. P. Zahn and J. Zinn-Justin, Proceedings of the Les Houches Summer School on Astrophysical Fluid Dynamics, XLVII, 1987 (Elsevier, Amsterdam, 1993).
[36] U. Frisch *et al.*, J. Fluid Mech. **68**, 769 (1975).
[37] A. Brandenburg and K. Subramanian, Phys. Rep. **417**, 1 (2005).
[38] P. D. Mininni *et al.*, Parallel Comput. **37**, 316 (2011).
[39] M. E. Brachet *et al.*, J. Fluid Mech. **130**, 411 (1983).
[40] C. Cichowlas, P. Bonaiti, F. Debbasch, and M. Brachet, Phys. Rev. Lett. **95**, 264502 (2005).
[41] H. Politano, A. Pouquet, and P. L. Sulem, Phys. Plasmas **2**, 2931 (1995).
[42] C. Bardos, M. C. Lopes Filho, D. Niu, H. J. Nussenzveig Lopes, and E. S. Titi, arxiv:1201.2742.
[43] W. H. Matthaeus, A. Pouquet, P. D. Mininni, P. Dmitruk, and B. Breech, Phys. Rev. Lett. **100**, 085003 (2008).
[44] A. Pouquet, U. Frisch, and J. Léorat, J. Fluid Mech. **77**, 321 (1976).
[45] K. T. Osman *et al.*, Astrophys. J. **741**, 75 (2011).
[46] J. Stawarz *et al.*, Astrophys. J. **697**, 1119 (2009).
[47] J. Stawarz *et al.*, Astrophys. J. **713**, 920 (2010).
[48] L. Sorriso-Valvo, R. Marino, V. Carbone, A. Noullez, F. Lepreti, P. Veltri, R. Bruno, B. Bavassano, and E. Pietropaolo, Phys. Rev. Lett. **99**, 115001 (2007).
[49] R. Marino *et al.*, Astrophys. J. **677**, L71 (2008).
[50] G. Ivey, K. Winters, and J. Koseff, Annu. Rev. Fluid Mech. **40**, 169 (2008).
[51] G. Falkovich, J. Phys. A: Math. Theor. **42**, 123001 (2009).